

An accurate two-phase approximate solution to an acute viral infection model

Amber M. Smith · Frederick R. Adler · Alan S. Perelson

Received: 16 April 2009 / Revised: 25 June 2009
© Springer-Verlag 2009

Abstract During an acute viral infection, virus levels rise, reach a peak and then decline. Data and numerical solutions suggest the growth and decay phases are linear on a log scale. While viral dynamic models are typically nonlinear with analytical solutions difficult to obtain, the exponential nature of the solutions suggests approximations can be found. We derive a two-phase approximate solution to the target cell limited influenza model and illustrate its accuracy using data and previously established parameter values of six patients infected with influenza A. For one patient, the fall in virus concentration from its peak was not consistent with our predictions during the decay phase and an alternate approximation is derived. We find expressions for the rate and length of initial viral growth in terms of model parameters, the extent each parameter is involved in viral peaks, and the single parameter responsible for virus decay. We discuss applications of this analysis in antiviral treatments and in investigating host and virus heterogeneities.

Keywords Acute virus infection · Influenza · Virus dynamics model · Approximation of nonlinear differential equations

Mathematics Subject Classification (2000) 92B05 · 37N25

A. M. Smith (✉)
Department of Mathematics, University of Utah, Salt Lake City, UT 84112, USA
e-mail: smith@math.utah.edu

F. R. Adler
Departments of Mathematics and Biology, University of Utah, Salt Lake City, UT 84112, USA

A. S. Perelson
Theoretical Biology and Biophysics Group, Theoretical Division,
Los Alamos National Laboratory, Los Alamos, NM 87545, USA

1 Introduction

Mathematical models have been used to study the infection kinetics of viruses, such as HIV, hepatitis B and C, and influenza, and have resulted in estimation of such quantities as *in vivo* viral replication rates, virus half-lives and infected cell life-spans (Baccam et al. 2006; Ho et al. 1995; Lewin et al. 2001; Neumann et al. 1998; Nowak et al. 1996; Perelson et al. 1997, 1996). These models are frequently nonlinear and analysis is usually limited to parameter estimation and numerical simulation. Approximate analytically tractable solutions could provide easier interpretation of virus dynamics and identify the extent to which each parameter influences infection kinetics including viral rise, peak and decay and the associated time scales.

The basic model structure (Eqs. (1)–(3)), summarized in Nowak and May (2001) and Perelson (2002), describes a viral infection using three state variables: target cells (T), infected cells (I), and free virus (V).

$$\frac{dT}{dt} = s - dT - \beta TV \quad (1)$$

$$\frac{dI}{dt} = \beta TV - \delta I \quad (2)$$

$$\frac{dV}{dt} = pI - cV \quad (3)$$

In Eqs. (1)–(3), uninfected cells are supplied at constant rate s , die at rate d and become infected at rate βV . Infected cells are lost, either to apoptosis or removal by immune cells, at rate δ . Virion production occurs at rate p per cell and virions are cleared at rate c per day.

Virus initially grows exponentially while the target cell population remains relatively constant (Fig. 1). Nowak et al. (1997) found if T is constant, then viral growth occurs according to $e^{r_0 t}$, where r_0 is the leading eigenvalue which solves $r_0^2 + (c + \delta)r_0 - c\delta(R_0 - 1) = 0$. Here, $R_0 = \beta ps / (c\delta d)$ is the basic reproductive number, which describes how many infected cells are produced per infected cell at the initiation of infection.

Following the initial exponential growth phase, virus levels reach a peak and then virus begins to slowly decrease. Target cells decline sharply, and the infected cell population peaks (Fig. 1). If target cell regeneration (s) is not considered, then following the peak virus asymptotically decays as $e^{-\delta t}$ and the infection is cleared. On the other hand, if s is large, then following the peak a short period of viral decay takes place before a steady state is reached (Bonhoeffer et al. 1997; Stafford et al. 2000).

Viral dynamics models have largely been applied to persistent infections; however, the basic model has also been used to study an influenza A virus (IAV) infection. Baccam et al. (2006) and Handel et al. (2007) applied simple target cell limited models to human nasal wash data collected daily from six individuals infected with IAV. Influenza is an acute infection usually lasting 7–10 days; therefore, some modifications of the basic model were made in their analyses. They first generalized the basic model to a model that included an eclipse phase to describe the time it takes for an infected cell to produce virions after it is initially infected. As previously done in HIV models

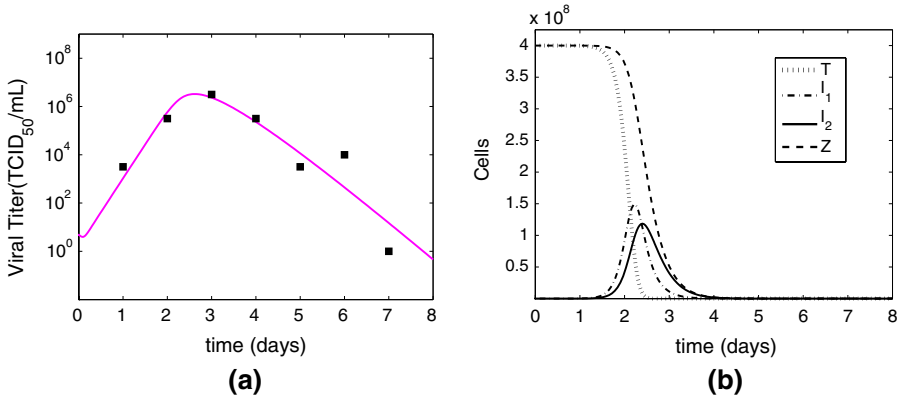


Fig. 1 Numerical solution of Eqs. (4)–(7) using Patient 4’s parameters (Table 1) and data (boxes). **a** Free virus (V), given in \log_{10} TCID₅₀/mL of nasal wash. **b** Cell populations: target cells (T , dotted line), infected cells not yet producing virus (I_1 , dash-dotted line), productively infected cells (I_2 , solid line), and total cells ($Z = T + I_1 + I_2$, dashed line)

(Perelson et al. 1993), infected cells were split into two class: I_1 , representing infected cells that have not yet begun producing virions and I_2 , representing infected cells that are producing virus. Transition from I_1 to I_2 is assumed to occur at rate k with no death occurring before virus production begins. Productively infected cells are lost at rate δ . Lastly, the models did not consider processes which have longer time scales, such as natural cell death ($d = 0$). The source of new target cells, s , was also set to zero as little epithelial cell regeneration occurs before virus is cleared, and estimates of s based on data fitting were indistinguishable from zero (Baccam et al. 2006). This target cell limited model (with $s = 0, d = 0$) is described by Eqs. (4)–(7) and is the focus of our work.

$$\frac{dT}{dt} = -\beta TV \tag{4}$$

$$\frac{dI_1}{dt} = \beta TV - kI_1 \tag{5}$$

$$\frac{dI_2}{dt} = kI_1 - \delta I_2 \tag{6}$$

$$\frac{dV}{dt} = pI_2 - cV. \tag{7}$$

Baccam et al. (2006) fit Eqs. (4)–(7) to estimate parameter values for all six patients. The dynamics are shown in Fig. 1, which plots free virus (panel (a)) and each cell population (panel (b)) against time. Values for parameters β, p, k, c, δ , the initial viral titer, V_0 , and the basic reproductive ratio, R_0 , estimated by Baccam et al. (2006) are provided in Table 1. For this model,

$$R_0 = \frac{\beta p T_0}{c \delta}, \tag{8}$$

Table 1 Estimates of parameter values for the target cell limited model with an eclipse phase, Eqs. (4)–(7), using nasal wash data of six patients infected with IAV taken from [Baccam et al. \(2006\)](#)

Patient	V_0	β	p	k	c	δ	R_0
1	4.3×10^{-2}	4.9×10^{-5}	2.8×10^{-2}	3.9	4.3	4.2	30.4
2	3.1×10^{-7}	1.1×10^{-3}	2.1×10^{-2}	2.0	11.0	10.9	75.0
3	7.0×10^{-1}	1.7×10^{-4}	3.0×10^{-3}	4.9	2.2	2.3	39.6
4	4.9	5.3×10^{-6}	1.3×10^{-1}	4.0	3.8	3.8	19.1
5	1.7	2.7×10^{-6}	5.9×10^{-1}	6.0	13.5	13.5	3.5
6	2.4	8.4×10^{-6}	7.1×10^{-2}	4.4	3.7	3.8	16.6

The best-fit initial viral titer (V_0 , TCID₅₀/mL), infection rate constant (β , (TCID₅₀/mL)⁻¹d⁻¹), transition rate for infected cells to produce virus (k , d⁻¹), death rate of infected cells (δ , d⁻¹), viral release rate per infected cell (p , (TCID₅₀/mL)d⁻¹), viral clearance rate (c , d⁻¹), and basic reproductive number (R_0) are given for each patient. Initial condition of target cells (T) was kept fixed at 4×10^8 cells ($I_1, I_2 = 0$ initially). TCID₅₀ (50% tissue culture infectious dose) is the dose required to have cytopathic effects in 50% of cell cultures

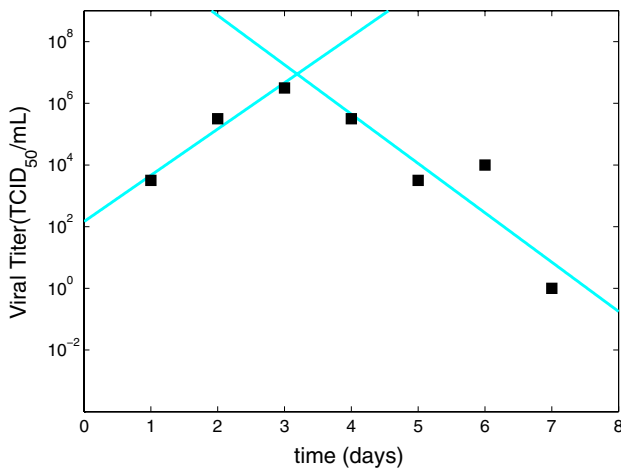


Fig. 2 Log-linear fits to data (Patient 4 from [Baccam et al. \(2006\)](#)) separating the initial virus rise (days 1–3) and subsequent virus decay (days 4–7). The number of data points included in each phase was found by finding which two lines produced the maximum likelihood fit

where $T(0) = T_0$ is the initial number of target cells, which was fixed at $T_0 = 4 \times 10^8$ based on an estimate of the number of epithelial cells in the upper respiratory tract.

For each patient, the viral dynamics break into two distinct phases that are linear on a log scale. As illustrated by Fig. 2, an initial period of exponential growth is followed by a phase of exponential decay, a behavior shown by the data and numerical solutions of the model. Understanding this characteristic behavior through analytical approximations is the central goal of this paper.

While Eqs. (4)–(7) are nonlinear and cannot be solved analytically, approximate solutions in each of the log-linear phases can be obtained. In this paper, we derive

these approximations for the initial viral growth phase and the subsequent viral decay phase. Using the data and parameters (Table 1) presented in Baccam et al. (2006), we verify the accuracy of the approximations. Finally, we use the approximate solutions to compare slopes and durations of growth and decay among the six patients in order to develop hypotheses about the host heterogeneity causing differences in dynamics.

2 Phase I approximate solution: initial viral growth

Phase I of acute viral infection kinetics is characterized by an initial dip in virus levels followed by exponential growth, as shown in Fig. 1. The dip occurs because virus is assumed to be continually lost, but there is a delay before virus production occurs. The exponential growth of virus is expected as long as the target cell level remains relatively constant because the system is linear when $T(t)$ is constant. The total number of cells, $Z(t) = T(t) + I_1(t) + I_2(t)$, during Phase I is also approximately constant (say, $Z \approx T_0$) as infected cells are at low levels during this phase, $Z \gg I_1 + I_2$. Throughout Phase I, target cells decline as they become infected eventually rendering this approximation inaccurate. A reduced system (Eqs. (9)–(11)) is obtained by using this approximation in Eqs. (4)–(7).

$$\frac{dI_1}{dt} = \beta T_0 V - k I_1 \tag{9}$$

$$\frac{dI_2}{dt} = k I_1 - \delta I_2 \tag{10}$$

$$\frac{dV}{dt} = p I_2 - c V. \tag{11}$$

Equations (9)–(11) are linear and can be solved. The characteristic equation is given by $\lambda^3 + B\lambda^2 + C\lambda + D = 0$ which has a discriminant, $\Delta = B^2C^2 - 4B^3D - 4C^3 + 18BCD - 27D^2$, that is less than zero since $B > 0, C > 0$ and $D < 0$. Therefore, we find one real (λ_1) and two complex ($\lambda_{2,3}$) eigenvalues with associated eigenvectors, $\xi_{1,2,3}$. Values of $\lambda_{1,2,3}$ for each patient are provided in Table 2.

Table 2 Values for all six patients of the eigenvalues, $\lambda_{1,2,3}$ (day^{-1}), in the Phase I solution, the final time (t_1 , days) the Phase I solution is valid, and the start time (t_2 or \tilde{t}_2 , days) of the Phase II solution

Patient	PHASE I			PHASE II	
	$\lambda_1(\text{d}^{-1})$	$\lambda_{2,3}(\text{d}^{-1})$	$t_1(\text{d})$	$t_2(\text{d})$	$\tilde{t}_2(\text{d})$
1	8.76	$-10.58 \pm 11.16i$	1.62	2.00	
2	18.83	$-21.37 \pm 22.63i$	1.26	1.44	
3	6.94	$-8.17 \pm 8.59i$	1.41	1.89	
4	6.46	$-9.04 \pm 8.95i$	1.76	2.28	
5	5.08	$-19.04 \pm 13.23i$	2.64		3.86
6	6.20	$-9.05 \pm 8.80i$	1.87	2.41	

$$\lambda_1 = \sqrt[3]{-\frac{q}{2} + \sqrt{\frac{q^2}{4} + \frac{u^3}{27}}} + \sqrt[3]{-\frac{q}{2} - \sqrt{\frac{q^2}{4} + \frac{u^3}{27}}} - \frac{B}{3}, \tag{12}$$

$$\lambda_{2,3} = \left(-\frac{1}{2} \pm i \frac{\sqrt{3}}{2}\right) \sqrt[3]{-\frac{q}{2} + \sqrt{\frac{q^2}{4} + \frac{u^3}{27}}} + \left(-\frac{1}{2} \mp i \frac{\sqrt{3}}{2}\right) \sqrt[3]{-\frac{q}{2} - \sqrt{\frac{q^2}{4} + \frac{u^3}{27}}} - \frac{B}{3}, \tag{13}$$

where

$$\begin{aligned} u &= C - \frac{B^2}{3} \\ q &= D + \frac{2B^3 - 9BC}{27} \\ B &= k + \delta + c, \\ C &= k\delta + kc + c\delta, \text{ and} \\ D &= -kc\delta(R_0 - 1). \end{aligned} \tag{14}$$

$$\xi_{1,2,3} = \begin{pmatrix} \xi_{11} \\ \xi_{12} \\ \xi_{13} \end{pmatrix}, \begin{pmatrix} \xi_{21} \\ \xi_{22} \\ \xi_{23} \end{pmatrix}, \begin{pmatrix} \xi_{31} \\ \xi_{32} \\ \xi_{33} \end{pmatrix}$$

with

$$\begin{aligned} \xi_{j1} &= 1, \\ \xi_{j2} &= \frac{(\lambda_j + k)(\lambda_j + c)}{\beta T_0 p}, \text{ and} \\ \xi_{j3} &= \frac{\lambda_j + k}{\beta T_0}. \end{aligned}$$

Using initial conditions $I_1(0) = I_2(0) = 0$ and $V(0) = V_0$, we obtain the Phase I solution,

$$T(t) = T_0 - I_1(t) - I_2(t) \tag{15}$$

$$I_1(t) = \kappa_1 e^{\lambda_1 t} + \kappa_2 e^{\lambda_2 t} + \kappa_3 e^{\lambda_3 t} \tag{16}$$

$$I_2(t) = \kappa_1 \xi_{12} e^{\lambda_1 t} + \kappa_2 \xi_{22} e^{\lambda_2 t} + \kappa_3 \xi_{32} e^{\lambda_3 t} \tag{17}$$

$$V(t) = \kappa_1 \xi_{13} e^{\lambda_1 t} + \kappa_2 \xi_{23} e^{\lambda_2 t} + \kappa_3 \xi_{33} e^{\lambda_3 t}, \tag{18}$$

with constants

$$\begin{aligned} \kappa_1 &= \frac{V_0(k + \lambda_2)(k + \lambda_1)}{(\lambda_3 - \lambda_1)(\lambda_3 - \lambda_2)} \\ \kappa_2 &= \frac{V_0 \beta T_0 p}{(\lambda_3 - \lambda_1)(\lambda_3 - \lambda_2)} \\ \kappa_3 &= -\frac{V_0 \beta T_0 (\lambda_1 + k + c + \lambda_2)}{(\lambda_3 - \lambda_1)(\lambda_3 - \lambda_2)}. \end{aligned}$$

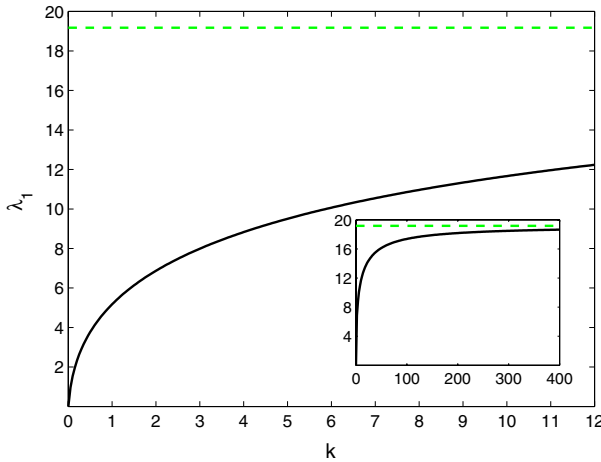


Fig. 3 The Phase I leading eigenvalue, λ_1 , over a range of values of the eclipse phase parameter, k . Also shown is the leading eigenvalue, r_0 , of the basic model with $s = 0$ and $d = 0$ (dashed line). As $k \rightarrow \infty$, λ_1 converges to r_0 (inset). Parameter values used were those of Patient 4 (Table 1)

The initial dip in virus levels can be attributed to λ_2 and λ_3 having negative real parts with magnitudes greater than λ_1 (Table 2). Following this, however, $e^{\lambda_2 t}$ and $e^{\lambda_3 t}$ decay leaving $e^{\lambda_1 t}$, which has positive real part, driving the exponential growth.

Ideally, we could identify a small number of parameters or parameter combinations that determine the slope of viral growth. However, the expression for λ_1 is complicated, and we cannot find any single parameter that has the most influence on this early phase. Using linear regressions, as in Fig. 2, can provide a rough estimate of λ_1 . Although specific parameters cannot be estimated by either the approximate solution or linear analysis, numerical exploration of each parameter indicates that all play large roles except for the initial virus concentration, V_0 .

We specifically looked at the sensitivity of λ_1 to the eclipse phase parameter, k . [Baccam et al. \(2006\)](#) found that including an eclipse phase gave more realistic parameter estimates than the simpler system without k , though the added complexity may not be statistically justifiable. The target cell limited model without k is equivalent to the basic model with $s = 0$ and $d = 0$, and the leading eigenvalue, r_0 , satisfies $r_0^2 + (c + \delta)r_0 - c\delta(R_0 - 1) = 0$, as discussed by [Nowak et al. \(1997\)](#) in the context of an HIV infection and [Lee et al. \(2009\)](#) in the context of an influenza infection. The resulting solution is $r_0 = -(c + \delta)/2 \pm \sqrt{(\delta - c)^2 + 4\beta p T_0}/2$. To compare the model with and without an eclipse phase, we plot λ_1 and r_0 versus k using the parameters of Patient 4 (Fig. 3). As expected, the calculated λ_1 from our analysis converges to r_0 as $k \rightarrow \infty$ (Fig. 3 inset). We also find that for k in biologically feasible ranges, e.g. $k \in [2, 6]$, small variations lead to significant changes in the slope of viral growth.

The Phase I solution is valid from $t = 0$ until some time $t = t_1$, which is defined to be the time for which T_0 is no longer a good approximation for $Z(t)$. We set this to occur when $T(t)$ has been depleted by $\sim 10\%$ of its initial value. This value is somewhat arbitrary; however, smaller values (5%) were not sufficient and larger values

(15%) began to result in large deviations of the approximations from the numerical solution. Therefore, t_1 solves $T(t_1) = 0.9T_0$. Terms involving exponentials of λ_2 and λ_3 can be ignored in the calculation of t_1 since $e^{\lambda_1 t}$ is the dominating term. Solving $0.9T_0 = T_0 - \kappa_1(1 + \xi_{12})e^{\lambda_1 t_1}$, we obtain the expression,

$$t_1 = \frac{\ln(0.1T_0) - \ln(\kappa_1) - \ln(1 + \xi_{12})}{\lambda_1}. \tag{19}$$

Using the parameters in Table 1, we calculated the value of t_1 for each patient (Table 2). Figure 4 illustrates the Phase I solution, numerical simulation of the target cell limited model, and t_1 for each of the six patients.

3 Phase II approximate solution: virus decay

Following the initial exponential rise in Phase I, viral growth begins to slow as target cells sharply decline. At this point, most remaining cells are infected since target cells are nearly depleted. This behavior characterizes Phase II of the infection kinetics; therefore, during this phase, $Z \gg T$ implying that $I_1 \approx Z - I_2$. Using this approximation in Eqs. (4)–(7) results in the reduced system

$$\frac{dI_1}{dt} = -kI_1 \tag{20}$$

$$\frac{dI_2}{dt} = kI_1 - \delta I_2 \tag{21}$$

$$\frac{dZ}{dt} = -\delta I_2 \tag{22}$$

$$\frac{dV}{dt} = pI_2 - cV. \tag{23}$$

We define t_2 to be the time at which the Phase II solution begins. Solving Eqs. (20)–(23) yields the expressions,

$$I_1(t) = I_1(t_2)e^{-k(t-t_2)} \tag{24}$$

$$I_2(t) = \frac{Z(t_2)k - I_2(t_2)\delta}{k - \delta} e^{-\delta(t-t_2)} + \frac{I_2(t_2) - Z(t_2)}{k - \delta} ke^{-k(t-t_2)} \tag{25}$$

$$Z(t) = \frac{Z(t_2)k - I_2(t_2)\delta}{k - \delta} e^{-\delta(t-t_2)} + \frac{I_2(t_2) - Z(t_2)}{k - \delta} \delta e^{-k(t-t_2)} \tag{26}$$

$$V(t) = \frac{p}{k - \delta} \left(\frac{Z(t_2)k - I_2(t_2)\delta}{c - \delta} e^{-\delta(t-t_2)} + \frac{I_2(t_2) - Z(t_2)}{c - k} ke^{-k(t-t_2)} \right) + V_s e^{-c(t-t_2)} \tag{27}$$

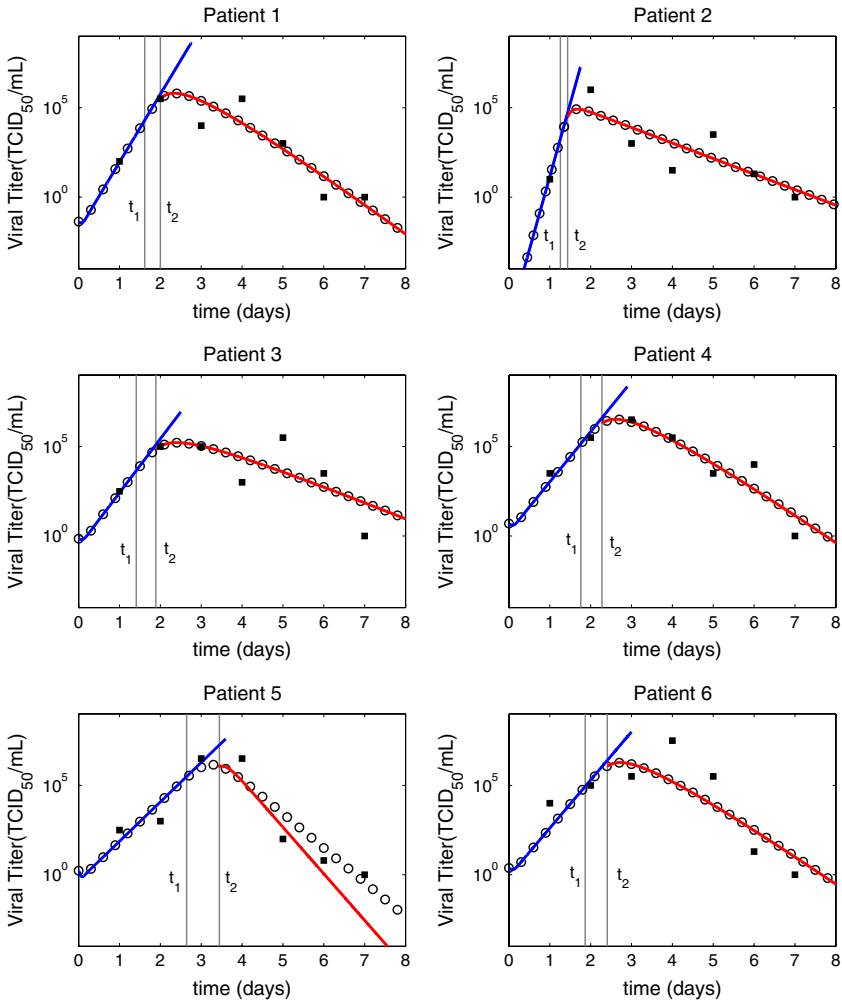


Fig. 4 Phase I and II virus (V) approximate solutions (*solid lines*) plotted against experimental data (*squares*) and fits (*circles*) of Eqs. (4)–(7) for all six patients. Virus titers are given in TCID₅₀/mL of nasal wash. The final time, t_1 , of the Phase I solution and the start time, t_2 , of the Phase II solution are given by vertical lines

where

$$V_s = V(t_2) - \frac{p}{k - \delta} \left(\frac{Z(t_2)k - I_2(t_2)\delta}{c - \delta} + \frac{I_2(t_2) - Z(t_2)}{c - k} \right).$$

This approximation is a combination of exponentials involving the parameters k , c and δ . This solution takes on a different form if $k = c$, $k = \delta$ and/or $c = \delta$, which can be obtained by appropriate use of l’Hôpital’s rule.

During Phase II, growth of free virus has slowed significantly and a peak is reached. From here, virus decline begins and becomes exponential. In the region around the peak, all three exponential terms are involved; however, the rate of asymptotic decay depends on the values of k , c and δ . If all three are similar in value, each contributes throughout much of the infection resolution with the smallest dominating towards the end. On the other hand, if one is much smaller than the other two, it will dictate the slope of viral decay. If we have an a priori hypothesis about which is smallest, the slope obtained from doing a linear fit (Fig. 2) provides an estimate of this parameter.

The Phase II solution is valid from $t = t_2$, the time at which $T(t)$ becomes sufficiently small, until infection resolution. We assumed that $T(t) \approx 0$ to find the approximate solution given by Eqs. (24)–(27). However, $T(t)$ is not identically equal to zero in the initial portion of this phase and is necessary to define t_2 . To derive an approximate solution for $T(t)$, we expand each state variable as a power series in ε and write, for example, $V(t) = V^{(0)} + \varepsilon V^{(1)} + O(\varepsilon^2)$. Because $T(t)$ is small in this phase, we assume $T(t) = \varepsilon T^{(1)} + O(\varepsilon^2)$, i.e., $T^{(0)} = 0$. The solution in Eqs. (24)–(27) is equivalent to substituting these expansions into Eqs. (4)–(7) and solving the zeroth order ($O(\varepsilon^0)$) subsystem. In the order ε ($O(\varepsilon^1)$) subsystem, we find that a solution for $T^{(1)}$ can be obtained by substituting Eq. (27) into $dT/dt = -\beta TV$ and integrating, yielding

$$T(t) = T(t_2)e^{-\beta \left\{ \frac{p}{k-\delta} \left[\frac{Z(t_2)k - I_2(t_2)\delta}{(c-\delta)\delta} (1 - e^{-\delta(t-t_2)}) + \frac{I_2(t_2) - Z(t_2)}{(c-k)k} k(1 - e^{-k(t-t_2)}) \right] + \frac{V_2}{c} (1 - e^{-c(t-t_2)}) \right\}} \tag{28}$$

The remaining order ε differential equations are a set of linear, non-autonomous equations that cannot be directly solved. However, numerically solving this subsystem, we find that the zeroth order approximation (Eqs. (24)–(27)) is nearly indistinguishable from the order ε solution for the other state variables, particularly $V(t)$.

We then set the time the Phase II solution begins to be when $T(t)$ is at 10% of its initial value ($T_0 = 4 \times 10^8$ cells). Again, we found that smaller values are not sufficient while larger values produced inaccuracy. We are not able to derive an expression for t_2 as we did for t_1 because initial values of the state variables (e.g. $Z(t_2)$) are unknown. There is a short time period where neither the Phase I nor the Phase II approximation is valid; therefore, we cannot use the values of state variables at the conclusion of Phase I for the initial value of Phase II. Because of this, a numerical method was used to find the value of t_2 that satisfies $T(t_2) = 0.1T_0 = 4 \times 10^7$ cells and the values of state variables at this time. Table 2 contains the calculated t_2 for each patient. These times are plotted in Fig. 4 along with the Phase II solution for all six patients.

3.1 An alternate Phase II approximate solution

The Phase II solution (Eqs. (24)–(28)) is accurate only if the number of target cells is small at some arbitrary time t_2 and continues to approach zero as $t \rightarrow \infty$. In the initial stages of this phase, free virus peaks and infected cells make up the majority

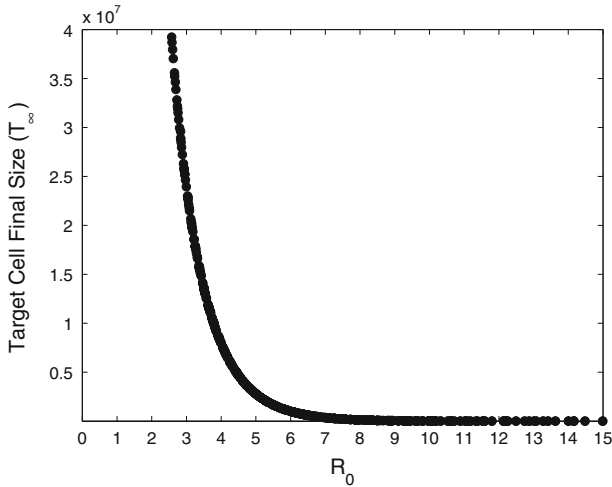


Fig. 5 Target cell final size, T_∞ , with the corresponding value of the basic reproductive number, R_0 , for various parameter combinations

of the total cell population (i.e. $T \ll I_1 + I_2 \approx Z$). This approximation continues throughout infection resolution so long as target cells continue to become infected. However, should free virus and/or infected cells be cleared too quickly for further infection of target cells to take place, then the total cell population will eventually consist mostly of susceptible cells (i.e. $Z \approx T \gg I_1 + I_2$).

Using the numerical solution, we found the final number of target cells as $t \rightarrow \infty$, denoted by T_∞ . With the estimated parameters, the value of T_∞ is zero cells for Patient’s 1, 2 and 3, two cells for Patient 4, and 17 cells for Patient 6. However, Patient 5 retains a significant number of cells, 1.37×10^7 cells, and therefore, the approximation of Phase II is initially valid but eventually fails (Fig. 4).

A dependence of the final number of target cells on R_0 was shown for the classic epidemic model by [Kermack and McKendrick \(1927\)](#) and later by [Diekmann and Heesterbeek \(2000\)](#). For the epidemic model, target cell final size was determined to satisfy $\ln(T_\infty/T_0) = R_0(T_\infty/T_0 - 1)$. The solution was found to be $T_\infty \approx T_0 e^{-R_0}$ for $R_0 \gg 1$. Because of the similarities between Eqs. (4)–(7) and the Kermack-McKendrick model, we find this equation to be a good approximation of T_∞ for the target cell limited model. Estimates of the target cell final size for each patient can then be easily calculated for a given value of R_0 , e.g. $T_\infty \approx 4 \times 10^8 e^{-19.1} = 2$ cells for Patient 4 and $T_\infty \approx 4 \times 10^8 e^{-3.5} = 1.21 \times 10^7$ cells for Patient 5.

We further examined R_0 (Eq. (8)) to determine when the Phase II solution becomes invalid. A plot of target cell final sizes, given different parameter combinations, and associated R_0 values revealed that low basic reproductive numbers result in significant levels of susceptible cells late in the infection (Fig. 5). The number of surviving target cells increases significantly for $R_0 < 7$ leading to failure of the approximation. For Patient 5, $R_0 = 3.5$ is significantly lower than that of the other five patients; therefore, an alternative approximation is needed.

In Phase I, we used the fact that the total number of cells (Z) remained relatively constant and that $Z \gg I_1 + I_2$ to derive an approximation. We find a similar behavior in Phase II as Z reaches a non-zero constant state when target cells are not fully depleted. We can then take advantage of the approximation used in Phase I to derive an alternate approximation for Phase II. Here, we have $T \approx T_\infty$ and define \tilde{t}_2 as the time that the alternate Phase II solution begins. This approximation results in the alternate solution being defined by $Z(t) = T_\infty + I_1 + I_2$ and Eqs. (16)–(18) but with T_∞ in place of T_0 and with constants,

$$\begin{aligned} \tilde{\kappa}_1 &= \frac{V(\tilde{t}_2)(k+\lambda_2)(k+\lambda_1)(\lambda_1-\lambda_2) - I_1(\tilde{t}_2)(k+\lambda_3)(k+\lambda_2)(\lambda_3-\lambda_2) + I_2(\tilde{t}_2)(k+\lambda_3)(k+\lambda_1)(\lambda_3-\lambda_1)}{(\lambda_1-\lambda_2)(\lambda_3-\lambda_2)(\lambda_3-\lambda_1)e^{\lambda_1\tilde{t}_2}} \\ \tilde{\kappa}_2 &= \frac{\beta T_\infty p [V(\tilde{t}_2)(\lambda_1-\lambda_2) - I_1(\tilde{t}_2)(\lambda_3-\lambda_2) + I_2(\tilde{t}_2)(\lambda_3-\lambda_1)]}{(\lambda_1-\lambda_2)(\lambda_3-\lambda_2)(\lambda_3-\lambda_1)e^{\lambda_2\tilde{t}_2}} \\ \tilde{\kappa}_3 &= -\frac{\beta T_\infty [V(\tilde{t}_2)(\lambda_1-\lambda_2)(\lambda_1+k+c+\lambda_2) - I_1(\tilde{t}_2)(\lambda_3-\lambda_2)(\lambda_2+k+c+\lambda_3) + I_2(\tilde{t}_2)(\lambda_3-\lambda_1)(\lambda_3+k+c+\lambda_1)]}{(\lambda_1-\lambda_2)(\lambda_3-\lambda_2)(\lambda_3-\lambda_1)e^{\lambda_3\tilde{t}_2}} \end{aligned}$$

The approximation is valid for a shorter time period ($\tilde{t}_2 > t_2$) than the previous Phase II solution. This will always be the case since the previous Phase II solution only requires target cells to be at low levels but not necessarily constant. In that instance, target cells are still changing with respect to time before they reach a constant steady state. On the other hand, the alternate solution does not begin until target cells have reached this constant state.

To calculate \tilde{t}_2 , we find the time at which T_∞ becomes a good approximation for $T(t)$. As with t_2 , we used numerical methods to determine the time when $T(\tilde{t}_2) - T_\infty = 25\% T_\infty = 1.71 \times 10^7$ cells. We tried larger values than 25% but found they were inadequate.

Using the parameters for Patient 5 (Table 1) and values of the state variables at \tilde{t}_2 , we find one real ($\lambda_1 = -4.42$) and two complex ($\lambda_{2,3} = -14.29 \pm 3.71i$) eigenvalues. Plugging T_∞ in for T_0 in Eq. (12) results in a negative value of λ_1 in the second phase since $R_0 = \beta p T_\infty / c \delta < 1$. While this solution does not capture the viral peak, information concerning the slope can still be obtained. As before, λ_1 dominates and defines the rate of viral decay. The alternate Phase II solution is plotted with t_1, \tilde{t}_2 and the numerical results in Fig. 6.

4 Discussion

We studied an acute virus infection model, specifically the target cell limited influenza model (Eqs. (4)–(7)), to find a two-phase approximate analytical solution. We focused on investigating the log-linear property of viral load data using human nasal wash data from six patients and their associated parameter values (Table 1), estimated in Baccam et al. (2006). Although the published estimates do not include confidence intervals on the parameters for individual patients, we use the estimated values to illustrate the accuracy of the approximations and to investigate the slopes and timing of virus growth and decay.

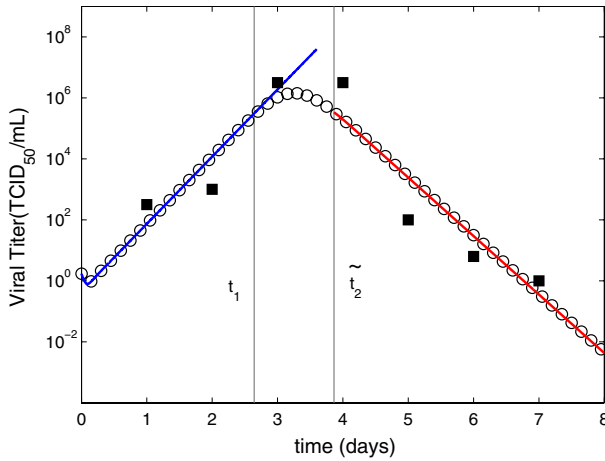


Fig. 6 Phase I and alternate Phase II virus (V) approximate solutions plotted against experimental data (squares) and fits (circles) of Eqs. (4)–(7) for Patient 5. Virus titers are given in TCID₅₀/mL of nasal wash. The final time, t_1 , of the Phase I solution and the start time, t_2 of the alternate Phase II solution are given by vertical lines

The initial phase, Phase I, is defined by target cells remaining relatively constant and lasts until approximately 10% of the target cells have been infected. During this phase, we found exponential viral growth to be driven by the leading eigenvalue, λ_1 , for a time t_1 (Table 2, Fig. 4). While we cannot extract one or two parameters controlling the value of this complicated expression, we can use the equation to evaluate differences among hosts or among virus strains.

We examined how changes in k , the eclipse phase parameter, affect the value of λ_1 because including an eclipse phase complicates the basic viral infection model but does not appear to change its characteristic behavior and may not be justified statistically (Baccam et al. 2006). We verified that λ_1 converges to the leading eigenvalue, r_0 , of the basic model as $k \rightarrow \infty$ (Fig. 3). However, for k in biologically realistic ranges, λ_1 is significantly lower than r_0 , given the same parameter values. This suggests that parameters will estimate to significantly different values with each of these models, a finding consistent with the conclusions made by Baccam et al. (2006). We also find that λ_1 is quite sensitive to k such that small changes in the eclipse phase length could lead to large changes in the rate of viral growth and, thus, produce distinct growth phases.

When parameter values have been estimated, we find the general trend that fast viral growth (large λ_1) results in rapid target cell depletion and an early peak (small t_1). Patient 2 had the largest λ_1 and, hence, a short Phase I lasting for only about 30 hours. In contrast, the smallest growth parameters belonged to Patient 5 whose exponential growth phase was twice as long.

This variability highlights the challenge in effectively prescribing influenza antivirals. Currently, the antiviral Tamiflu is recommended during the first 12–24 hours to ensure maximum efficacy (Aoki et al. 2003). In our analysis, the length of Phase I (t_1) may be an indication of the available window to treat a patient effectively. The

opportunity for antiviral administration may last longer in some patients (e.g. Patient 5) than in others (e.g. Patient 2).

We have not fully addressed the gap between Phases I and II. This middle phase is truly nonlinear, and we were unable to find a simple approximation. Although this intermediate phase is not necessary to understand the exponential nature of acute viral infections, it does remain a focus of future work.

In the final phase, Phase II, infection resolution takes place. In this phase, target cells have markedly declined and both infected cells and free virus have a peak followed by exponential decay. The rate of virus decay depends on the smallest of k , c and δ while the viral peak depends on all three of these parameters. This result is similar to that found for the basic model where virus was determined to asymptotically decline according to $e^{-\delta t}$ when $c \gg \delta$ (Bonhoeffer et al. 1997).

We believe that δ , the infected cell death rate, will often determine the rate of virus decay. This is not true for all infections since the eclipse phase length can vary from 4–6 hours for influenza to a day or more for human immunodeficiency virus (HIV) (Nelson et al. 2001; Dixit et al. 2004). However, for many acute infections, infected cells are reasonably long lived compared to both free virus and the eclipse phase length. For several patients, the parameter values predicted by Baccam et al. (2006) do not reflect this observation. One possible explanation is that parameter estimation schemes find it difficult to distinguish between k , c and δ as each contributes to the viral decay in the latter phase, leading them to estimate two or all three parameters to similar value. To remedy this, one could fit parameters constraining k and c to be larger than δ .

With $k \gg \delta$ and $c \gg \delta$, parameter estimation is not necessary to understand viral decay, and δ can be approximated by a linear fit such as that in Fig. 2. Additionally, the up slope obtained from fitting data in Phase I could be used to estimate λ_1 and to compare hosts and/or virus strains. This presents an opportunity for biologists to utilize the tools developed here in a simple manner.

There are other ways to compare virus strains without access to specific parameter values as well. For example, genetically engineered influenza strains which differ only in their hemagglutinin (the surface protein used in cell entry) may have similar parameter values except for different infectivity rates, β . Using reasonable choices for the other parameters, the behavior of each strain (i.e. how quickly and for how long virus levels rise) could still be tested. We can also determine the extent of damage to the epithelium and virus transmissibility without the need for parameter estimation. These quantities, in terms of the parameters, can be investigated by taking the integrals of $I_2(t)$ and $V(t)$ in each phase.

As illustrated in Fig. 4, the Phase II solution, given by Eqs. (24)–(28), does not agree with numerical results for Patient 5. There was not an obvious indication in the data or linear fit that this patient was significantly different in any way. However, plotting the change in target cells over time (not shown) revealed that a large number of these cells remained late in infection. A reasonable estimate of this value can be easily found by calculating $T_\infty \approx T_0 e^{-R_0}$. The estimated parameters for this patient indicate a much smaller value of the basic reproductive number, R_0 , than the other five patients and, therefore, a larger target cell final size. When parameters fall in ranges that produce an $R_0 \lesssim 7$ (Fig. 5), as with Patient 5, the Phase II solution fails and an

alternate approximation is required. We use a similar approach to that in Phase I to derive a solution which does allow for small R_0 's. This approximate solution (Fig. 6) begins at a later time than the previous Phase II solution and does not capture the viral peak. However, if one is only interested in this late phase of decay, this approximation can be used for all patients where information on the rate of viral decay lies once again in λ_1 .

In summary, we have derived approximate solutions to the two exponential phases of acute virus infection dynamics. The approximations and the techniques we used are not restricted to an influenza A virus infection and could be easily extended to other virus models. The tools we describe are intended to complement parameter estimation and numerical simulation typically used for analysis of virus dynamics; however, several aspects are also amenable to use by experimentalists. This simplified analysis presents an opportunity to uncover new virus properties, investigate the implications of various drug therapies and aid in the development of therapies customized to individual patients based on the initial course of an infection.

Acknowledgments This material is based upon work supported by the National Science Foundation under grant DMS-0354259 (AMS), the Modeling the Dynamics of Life Fund at the University of Utah and the 21st Century Science Initiative Grant from the James S. McDonnell Foundation (FRA). Portions were done under the auspices of the US Department of Energy under contract DE-AC52-06NA25396 and supported in part by NIH contract N01-AI-50020 and grants RR06555-17 and AI28433-18 (ASP).

References

- Aoki FY, Macleod MD, Paggiaro P, Carewicz O, El Sawy A, Wat C, Griffiths M, Waalberg E, Ward P (2003) Early administration of oral oseltamivir increases the benefits of influenza treatment. *J Antimicrob Chemother* 51(1):123–129
- Baccam P, Beauchemin C, Macken CA, Hayden FG, Perelson AS (2006) Kinetics of influenza A virus infection in humans. *J Virol* 80(15):7590–7599
- Bonhoeffer S, May RM, Shaw GM, Nowak MA (1997) Virus dynamics and drug therapy. *Proc Natl Acad Sci USA* 94(13):6971–6976
- Diekmann O, Heesterbeek JAP (2000) *Mathematical epidemiology of infectious diseases: model building, analysis and interpretation*. Wiley, New York
- Dixit NM, Markowitz M, Ho DD, Perelson AS (2004) Estimates of intracellular delay and average drug efficacy from viral load data of HIV-infected individuals under antiretroviral therapy. *Antivir Ther* 9:237–246
- Handel A, Longini IM Jr, Antia R (2007) Neuraminidase inhibitor resistance in influenza: assessing the danger of its generation and spread. *PLoS Comput Biol* 3(12):e240
- Ho DD, Neumann AU, Perelson AS, Chen W, Leonard JM, Markowitz M (1995) Rapid turnover of plasma virions and CD4 lymphocytes in HIV-1 infection. *Nature* 373(6510):123–126
- Kermack WO, McKendrick AG (1927) A contribution to the mathematical theory of epidemics. *Proc R Soc Lond Ser A* 115(772):700–721
- Lee HY, Topham DJ, Park SY, Hollenbaugh J, Treanor J, Mosmann TR, Jin X, Ward B, Miao H, Holden-Wiltse J, Perelson AS, Zand M, Wu H (2009) Simulation and prediction of the adaptive immune response to influenza A virus infection. *J Virol* 83(14):7151–7165
- Lewin S, Ribeiro RM, Walters T, Lau GK, Bowden S, Locarnini S, Perelson AS (2001) Analysis of hepatitis B viral load decline under potent therapy: complex decay profiles observed. *Hepatology* 34(5):1012–1020
- Nelson PW, Mittler JE, Perelson AS (2001) Effect of Drug efficacy and the eclipse phase of the viral life cycle on estimates of HIV viral dynamic parameters. *J Acquir Immune Defic Syndr* 26(5):405–412
- Neumann AU, Lam NP, Dahari H, Gretch DR, Wiley TE, Layden TJ, Perelson AS (1998) Hepatitis C viral dynamics in vivo and the antiviral efficacy of interferon-therapy. *Science* 282(5386):103–107

- Nowak MA, Bonhoeffer S, Hill AM, Boehme R, Thomas HC, McDade H (1996) Viral dynamics in hepatitis B virus infection. *Proc Natl Acad Sci USA* 93(9):4398–4402
- Nowak MA, Lloyd AL, Vasquez GM, Wiltout TA, Wahl LM, Bischofberger N, Williams J, Kinter A, Fauci AS, Hirsch VM, Lifson JD (1997) Viral dynamics of primary viremia and antiretroviral therapy in simian immunodeficiency virus infection. *J Virol* 71(10):7518–7525
- Nowak MA, May R (2001) *Virus dynamics: mathematical principles of immunology and virology*. Oxford University Press, New York
- Perelson AS (2002) Modelling viral and immune system dynamics. *Nat Rev Immunol* 2(1):28–36
- Perelson AS, Essunger P, Cao Y, Vesanen M, Hurley A, Saksela K, Markowitz M, Ho DD (1997) Decay characteristics of HIV-1-infected compartments during combination therapy. *Nature* 387(6629):188–191
- Perelson AS, Kirschner DE, De Boer R (1993) Dynamics of HIV infection in CD4⁺ T cells. *Math Biosci* 114:81–81
- Perelson AS, Neumann AU, Markowitz M, Leonard JM, Ho DD (1996) HIV-1 dynamics in vivo: virion clearance rate, infected cell life-span, and viral generation time. *Science* 271(5255):1582–1586
- Stafford MA, Corey L, Cao Y, Daar ES, Ho DD, Perelson AS (2000) Modeling plasma virus concentration during primary HIV infection. *J Theor Biol* 203(3):285–301